Topochemical Anionic Subunit Insertion Reaction for Constructing Nanoparticles of Layered Oxychalcogenide Intergrowth Structures

Charles H. Wood[1] and Raymond E. Schaak[1,2,3,*]

[1] *Department of Chemistry,* [2] *Department of Chemical Engineering, and* [3] *Materials Research Institute, The Pennsylvania State University, University Park, PA 16802, United States.*

E-mail: res20@psu.edu

ABSTRACT

Intergrowth compounds contain alternating layers of chemically distinct subunits that yield composition-tunable, synergistic properties. Synthesizing nanoparticles of intergrowth structures requires atomic-level intermixing of the subunits rather than segregation into the stable constituent phases. Here, we introduce an anionic subunit insertion reaction for nanoparticles that installs metal chalcogenide layers between metal oxide sheets. Anionic $[CuS]^-$ subunits from solution replace interlayer chloride anions from LaOCl to form LaOCuS topochemically with retention of crystal structure and morphology. Sodium acetylacetonate helps extract Cl^- concomitant with the insertion of S^{2-} and Cu^+ and is generalized to other oxychalcogenides. This topochemical reaction produces nanoparticles of ordered mixed-anion intergrowth compounds and expands nanoparticle ion exchange chemistry to anionic subunits.

Colloidal nanoparticles are typically synthesized through direct solution-based methods where appropriate reagents are chemically and/or thermally triggered to react, which induces particle nucleation and growth.[1,2] However, for complex compositions and structures, including mixed-cation and mixed-anion intergrowth compounds that combine two or more distinct structural motifs, competition occurs between forming nanoparticles of simpler constituent compounds versus combining them into a single phase.[3,4] The family of intergrowth compounds *Ln*OCu*Ch* (*Ln* = lanthanide, *Ch* = chalcogen) provides an instructive example.[4-11] LaOCuS, for example, has alternating $[LaO]^+$ and $[CuS]^-$ layers. Forming LaOCuS requires atomic-level intermixing of these oxide and sulfide layers rather than forming separate La_2O_3 and copper(I) sulfide phases, which are both synthetically accessible.[12,13] As a result, LaOCuS and related compounds are not readily synthesized as nanoparticles using direct colloidal methods, although nanoparticulate powders can be made solvothermally under pressure and bulk powders through solid-state reactions.[10,14] More generally, intergrowth structures are difficult to synthesize colloidally, despite their growing interest across a wide range of applications.[3]

Topochemical methods locally modify composition and structure while maintaining the overall structural framework, making them ideally suited to intergrowths like LaOCuS, if precursors with related layered crystal structures and appropriate chemical reactivities can be found.[15,16] Topochemical reactions driven by acid-base and electrostatic interactions are common for bulk solids and include intercalation, deintercalation, and ion exchange.[17-19] Topochemical insertion of structural subunits to make intergrowths is also possible in bulk solids. For example, layered perovskite oxides with interlayer alkali metal cations undergo metathesis reactions with halide salts to form perovskite/halide intergrowths, such as the reaction of $RbLaNb_2O_7$ with $CuCl_2$ to produce $(CuCl)LaNb_2O_7$.[20] Topochemical manipulations of nanoparticles have primarily focused on cation and anion exchange, which use complex formation and differences in solvation energies and solubilities to drive cations or anions out of the solid, facilitating their replacement with other cations or anions from solution.[21-24] Expanding such capabilities to the insertion of structural subunits within a nanoparticle is important for increasing the compositional and structural complexity of synthetically accessible nanoparticles.

Here, we introduce a topochemical anionic subunit insertion reaction for nanoparticles that produces intergrowth compounds of metal oxides and sulfides. *Ln*O*X* (*X* = halogen) oxyhalides, which can be synthesized as nanoparticles, are structurally related to the *Ln*OCu*Ch* oxychalcogenides; both contain layers of $[LaO]^+$ that are separated by Cl^- or $[Cu\mathit{Ch}]^-$, respectively (Figure 1a).[6,25-28] We show that layers of $[CuS]^-$ can replace the interlayer Cl^- anions in LaOCl to form LaOCuS, facilitated by sodium acetylacetonate in solution that helps extract chlorine.

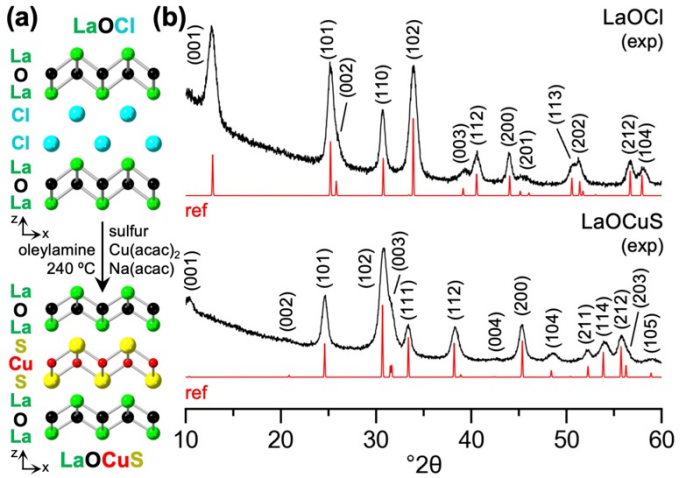

Figure 1. (a) Topochemical construction of LaOCuS from LaOCl. (b) Experimental and reference[12,13] XRD patterns for LaOCl and LaOCuS nanoparticles.

We synthesized LaOCl nanoparticles by thermally decomposing $LaCl_3 \cdot 7H_2O$ in oleylamine.[25] Powder XRD confirms their formation (Figure 1b). The increased relative intensities of the {00*l*} reflections indicates preferred orientation, suggesting a plate-like morphology.[25-28] The highlighted regions of the EDS spectrum in Figure 2a indicate the presence of lanthanum and chlorine. The HAADF-STEM image in Figure 2b shows that the LaOCl nanoparticles are polydisperse with average dimensions ranging from approx. 5–30 nm (Figure S1) and suggest a plate-like morphology, based on how some particles overlap; this observation is consistent with the preferred orientation indicated by XRD. Corresponding STEM-EDS element maps show colocalization of the La (57%) and Cl (43%) signals (Figure 2b, S2) and a composition (normalized to La) of $LaO_{1.12}Cl_{0.76}$ (Table S2). (Oxygen quantification, which is unreliable due to overlapping low-energy signals and large ambient background, was estimated based on charge balance.) The single-particle STEM-EDS element map in Figure 2b shows that the La signal extends to the surface but the Cl signal does not, suggesting a La-rich shell on LaOCl. XPS revealed that the surface contained (in addition to carbon) La (5%), O (15%), and Cl (5%) (Figure S3), indicating that it is rich in surface oxides.[31,32] Given their small particle sizes, XPS cannot unambiguously determine if chloride or oxide is on the surface versus buried within the particle. However, based on the combined data, we estimate that on average, a particle of “LaOCl” really contains only ~50% LaOCl, with the other ~50% corresponding to a shell of surface oxides and adsorbed chloride. This analysis is important for targeting the stoichiometry of the topochemical transformation that follows, as we assume that LaOCl is the only topochemically reactive component.

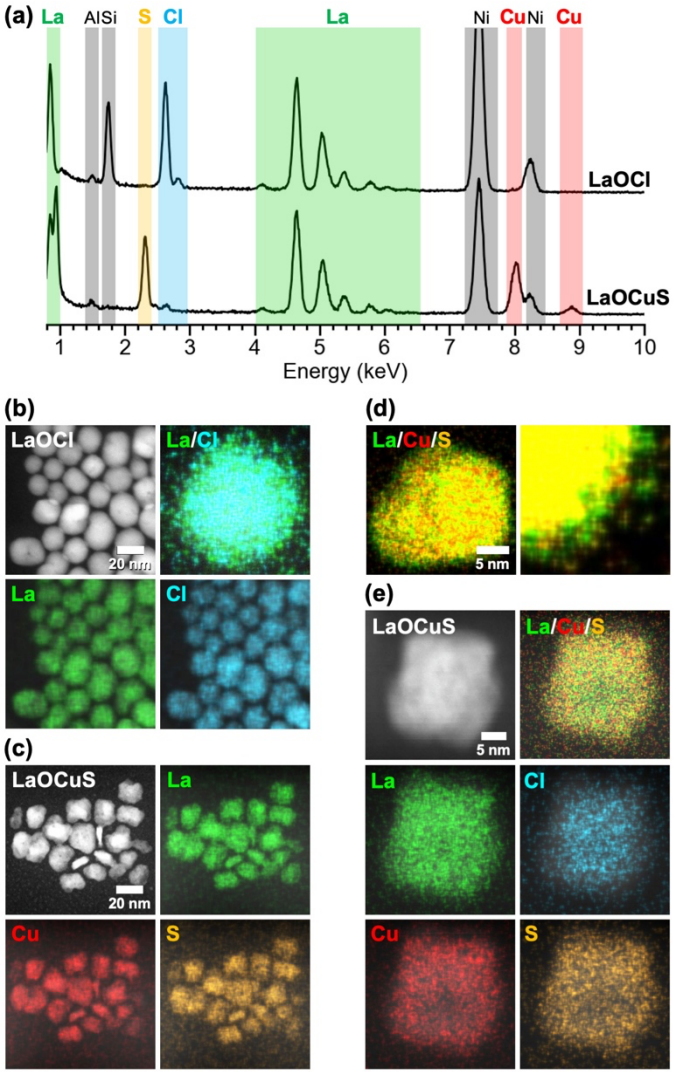

Figure 2. (a) EDS spectra highlighting the constant La, decreasing Cl, and increasing S signals upon transforming LaOCl to LaOCuS. Al and Si are adventitious and Ni is from the TEM grid. HAADF-STEM images and STEM-EDS element maps of (b) LaOCl nanoparticles (collection and single particle), (c) LaOCuS nanoparticles, (d) a single LaOCuS particle (including an enlarged surface region), and (e) partially-formed LaOCuS (after 15 minutes), showing a LaOCl-rich core.

To transform LaOCl to LaOCuS, an oleylamine solution containing $Cu(acac)_2$, sulfur powder, and Na(acac) was injected at 240 ºC into a suspension of LaOCl nanoparticles in oleylamine and held for 1 hour (Figure S4, S5). This reaction reduced Cu^{2+} to Cu^{1+} and sulfur to S^{2-} *via* oleylamine, as is well established for the synthesis of copper(I) sulfide nanoparticles.[33,34] The molar ratio of $Cu(acac)_2$ was chosen based on the analysis that only ~50% of the template particles consisted of LaOCl. Na(acac) and sulfur were chosen to be stoichiometric with the Cl in LaOCl. XRD data (Figure 1b) confirms the formation of LaOCuS and indicates preferred orientation along {00*l*}, which is crystallographically analogous to the preferred orientation in LaOCl and therefore

suggests retention of the plate-like morphology; the presence of (*hkl*) reflections rules out exfoliation. The HAADF-STEM image in Figure 2c shows that the morphologies and size distributions (~5-30 nm) of the LaOCuS particles are similar to those of LaOCl, consistent with a topochemical reaction. The corresponding STEM-EDS element maps confirm the homogeneous co-localization of La (44%), Cu (27%), and S (26%), as well as only a small amount (~3%) of residual Cl (Figure S6) at near-background levels, indicating removal of Cl (Table S3). The single-particle STEM-EDS element map in Figure 2d shows that the surface oxide that was present on LaOCl remains in LaOCuS; copper and sulfur signals are significantly lower than the lanthanum signal near the surface. EDS quantification indicates a composition of $LaOCu_{0.62}S_{0.59}$, which is close to the Cu:La ratio used in the reaction (Table S3) and corresponds roughly to $(LaO_x)_{0.4}$@$(LaOCuS)_{0.6}$ core-shell particles. XPS data also indicates an oxide-rich surface containing La (14%), O (38%), Cu (4%), S (6%) (Figure S7) with oxidation states of La^{3+}, Cu^{1+}, O^{2-}, and S^{2-}, consistent with literature XPS data for LaOCuS;[35-37] Cl is at background levels. When the reaction is stopped early, the amount of residual Cl is greater than at the full 60-minute reaction time (Figure 2e, S8, S9; Table S4, S5). The STEM-EDS element maps in Figure 2e for a product isolated at 15 minutes suggest that LaOCuS surrounds a LaOCl-rich core, which is consistent with a diffusion pathway that proceeds inward from the particle surface.

The UV-visible absorption spectra of LaOCl and LaOCuS nanoparticles are shown in Figure 3a. The corresponding Tauc plot for LaOCuS (Figure 3b) indicates a direct band gap of 3.19 eV, which matches well with the literature value of 3.14 eV for bulk LaOCuS.[38,39] The absorption feature at 308 nm is present and unchanged in both LaOCl and LaOCuS, and therefore is attributed to the persistent lanthanum oxide shell, based on the XPS data in Figure S7.[40] Colloidal suspensions of the LaOCl and LaOCuS nanoparticles appear colorless (Figure S10), as expected based on their literature band gaps.[6,10,11,41] In contrast, the product made using half-stoichiometric $Cu(acac)_2$ (as a control) is yellow, which corresponds to unreacted sulfur and is consistent with $Cu(acac)_2$ as the limiting reagent (Figure S10). The product made using double-stoichiometric $Cu(acac)_2$ (as a control) is brown with a broad NIR plasmon band (Figure 3c) that is consistent with copper(I) sulfide nanoparticles,[42,43] which form competitively with LaOCuS when too much $Cu(acac)_2$ is present. The enlarged plot in Figure 3d confirms identical behavior for all samples in the UV-Vis region where LaOCuS absorbs. The corresponding XRD pattern for the control sample made using double-stoichiometric $Cu(acac)_2$ includes both LaOCuS and $Cu_{1.8}S$ (Figure S11) while STEM-EDS maps show LaOCuS@LaOCl particles (Figure 3e, S12) and separate regions of copper sulfide (Figure 3f). These self-consistent observations by UV-Vis, XRD, and STEM-EDS indicate a competition between the topochemical reaction that transforms LaOCl to LaOCuS and a different reaction that forms copper sulfide, which can be mitigated by controlling stoichiometry.

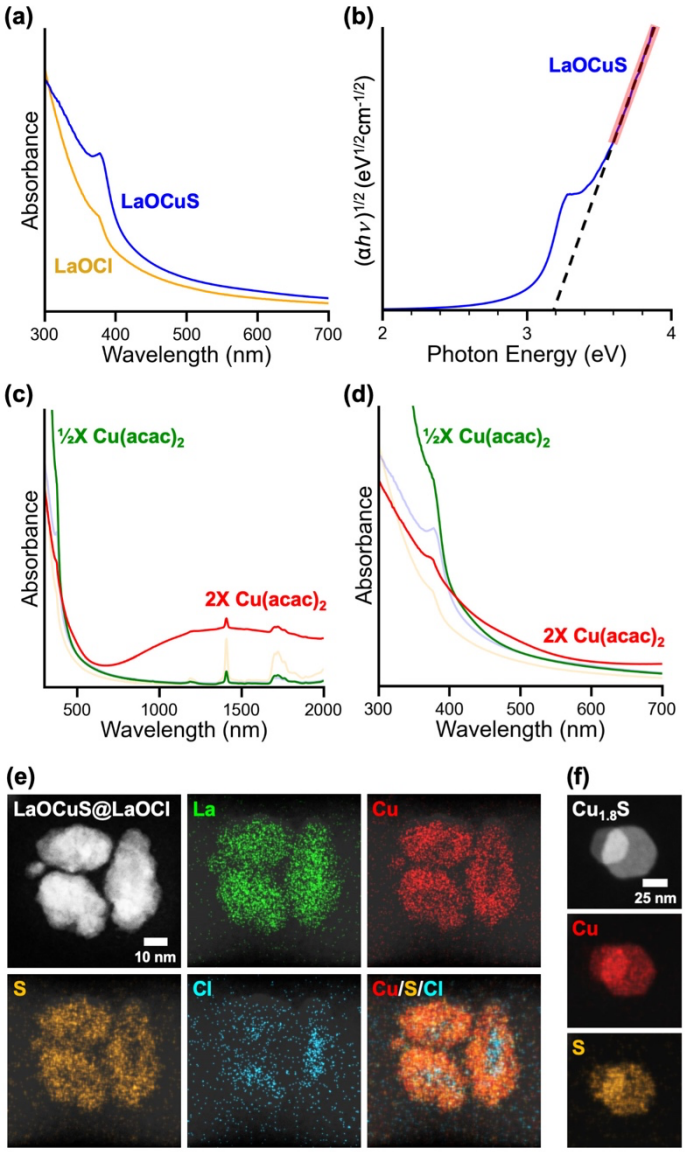

Figure 3. (a) UV-Vis absorbance spectra for LaOCl and LaOCuS. (b) Tauc plot for LaOCuS. (c,d) UV-Visible absorbance spectra for reactions that transform LaOCl (yellow) to LaOCuS (blue) using half (green) and twice (red) the normal amount of $Cu(acac)_2$. HAADF-STEM image and corresponding STEM-EDS element maps for (e) LaOCuS@LaOCl and (f) $Cu_{1.8}S$ particles, both observed in the double-stoichiometry $Cu(acac)_2$ reaction.

The data above provided evidence for a topochemical reaction by showing that the average size distribution and morphology of the precursor, as well as the lanthanum oxide shell (which is intrinsic to LaOCl and not part of the reaction), persist unchanged in the product. We further probed how chemical reactivity contributes to facilitating and driving the reaction. When CuCl and $CuCl_2$ were used instead of $Cu(acac)_2$, the reaction did not proceed, instead forming $Cu_{1.8}S$ and

unreacted LaOCl (Figure S13). The reaction also does not proceed if the copper and sulfur reagents are excluded (Figure S14, Table S6). When Na(acac) was removed from the reaction of LaOCl with $Cu(acac)_2$ and sulfur powder, the only product was $Cu_{1.8}S$ and unreacted LaOCl (Figure S13). Likewise, the reaction did not proceed when replacing Na(acac) with other sodium or acetylacetonate salts (Figure S15). This observation is crucial and unexpected, as it identifies Na(acac) as a key reagent necessary to transform LaOCl into LaOCuS, despite the absence of Na in the product. We propose that Na(acac) provides the driving force for removing Cl^- from LaOCl by coordinating the outgoing Cl^-, given the 1:1 Na^+:Cl^- stoichiometry and charge balance considerations along with knowledge that metal acetylacetonates can sometimes coordinate chloride.[44] The Cl^- is concurrently replaced by S^{2-} concomitant with insertion of Cu^+, which fills the tetrahedral holes to balance charge. Consistent with this hypothesis, analysis of STEM-EDS maps indicates decreasing chlorine signal in the nanoparticles as reaction time increases (Figures S8,S9; Tables S4,S5). Lack of reactivity when copper chloride salts are used is also consistent, as excess chloride would competitively bind Na(acac) and remove the driving force for Cl^- extraction from LaOCl. Sodium and chloride are not observed by STEM-EDS in the isolated products, NaCl is not observed by XRD, and Na and Cl are absent by XPS (Figure S7, S16).

This topochemical transformation is generalizable beyond LaOCuS. Reacting LaOCl with $Cu(acac)_2$, dibenzyl diselenide, and Na(acac) at 310 ºC for 1 hour forms the selenide analogue, LaOCuSe, as shown by XRD (Figure 4a). STEM-EDS element maps confirm the homogeneous co-localization of La (45%), Cu (28%), and Se (27%) and absence of Cl (Figure 4b, S17). EDS quantification indicates a composition of $LaOCu_{0.67}Se_{0.60}$ (Table S7), which includes LaOCuSe with a shell rich in lanthanum and oxygen. We also synthesized PrOCl and similarly transformed it to PrOCuS, as confirmed by XRD (Figure 4c, S18). STEM-EDS maps of PrOCl show colocalization of Pr (58%) and Cl (42%) (Figure S19) that correspond to a composition of $PrO_{1.14}Cl_{0.73}$ (Table S8), suggesting a shell rich in praseodymium and oxygen that is analogous to the lanthanum oxide shell on LaOCl. After the reaction is complete, STEM-EDS element maps of PrOCuS confirm the homogeneous co-localization of Pr (45%), Cu (27%), and S (24%) as well as only a small amount (~4%) of residual Cl (Figure 4d, S20). The composition of $PrOCu_{0.62}S_{0.54}$ (Table S9), *i.e.*, $(PrO_x)_{0.3}$@$(PrOCuS)_{0.7}$, is analogous to that observed for LaOCuS.

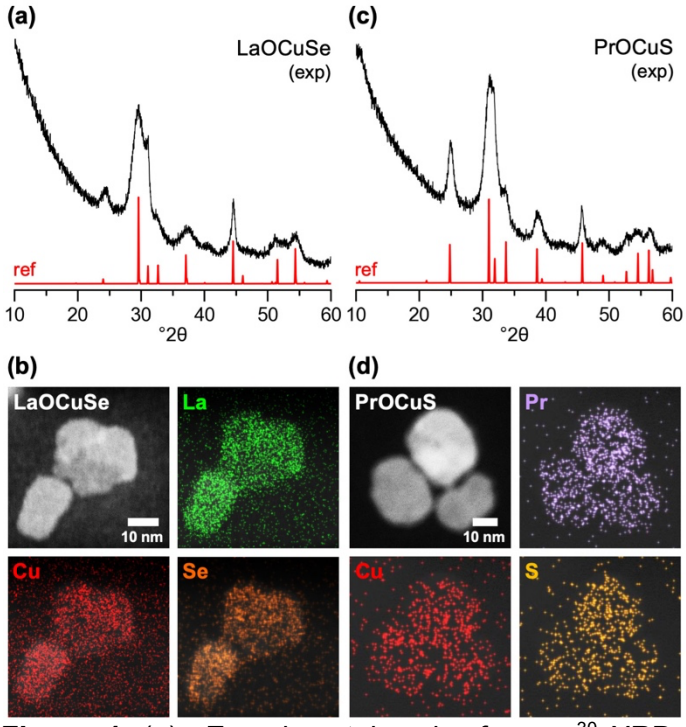

Figure 4. (a) Experimental and reference[30] XRD patterns and (b) HAADF-STEM image and STEM-EDS element maps for LaOCuSe nanoparticles. (c) Experimental and reference[45] XRD patterns and (d) HAADF-STEM image and STEM-EDS element maps for PrOCuS nanoparticles.

We topochemically transformed nanoparticles of *Ln*OCl to *Ln*OCu*Ch* through an anion subunit insertion reaction that exchanges interlayer Cl^- with $[CuS]^-$ and is facilitated by Na(acac) helping to drive chloride removal. This reaction expands nanoparticle ion exchange chemistry to include more compositionally and structurally complex systems containing interleaved anion/cation subunits while sidestepping competing reactions that result in phase segregation. Given the availability of nanoparticles that adopt similar structures to *Ln*OCl, including Bi*OX*, and a large number of stable and metastable *Ln*OCu*Ch* and BiOCu*Ch* compounds,[11,46] this reaction has the potential to produce nanoparticles of previously inaccessible photocatalysts, superconductors, semiconductors, thermoelectrics, and other useful materials.

ASSOCIATED CONTENT

Supporting Information

The Supporting Information is available free of charge on the ACS Publications website.

- Complete experimental details, additional STEM-EDS maps, quantification of EDS data, XRD data, XPS data, and UV-Visible spectroscopy data.

AUTHOR INFORMATION

Corresponding Author

Raymond E. Schaak – *Department of Chemistry*, *Department of Chemical Engineering*, and *Materials Research Institute*, *The Pennsylvania State University, University Park, Pennsylvania 16802, United States*; Email: res20@psu.edu

Authors

Charles H. Wood – *Department of Chemistry*, *The Pennsylvania State University, University Park, Pennsylvania 16802, United States*

Notes

The authors declare no competing financial interest.

ACKNOWLEDGMENT

This work was supported by the U.S. National Science Foundation under grant DMR-2210442. TEM, XRD, XPS, and UV-Visible spectroscopy data were acquired at the Materials Characterization Lab of the Penn State Materials Research Institute. The authors thank Dr. Jeff Shallenberger for help with XPS data collection and analysis.

REFERENCES

(1) Yin, Y.; Alivisatos, A. P. Colloidal Nanocrystal Synthesis and the Organic–Inorganic Interface. *Nature* **2004**, *437* (7059), 664–670.

(2) Buck, M. R.; Schaak, R. E.; Emerging Strategies for the Total Synthesis of Inorganic Nanostructures. *Angew. Chem., Int. Ed.* **2013**, *52* (24), 6154–6178.

(3) Larquet, C.; Carenco, S. Metal Oxysulfides: From Bulk Compounds to Nanomaterials. *Front. Chem.* **2020**, *8*, 179.

(4) Kageyama, H.; Hayashi, K.; Maeda, K.; Attfield, J. P.; Hiroi, Z.; Rondinelli, J. M.; Poeppelmeier, K. R. Expanding Frontiers in Materials Chemistry and Physics with Multiple Anions. *Nat. Comm.* **2018**, *9* (1), 1–15.

(5) Luu, S. D. N.; Vaqueiro, P. Layered Oxychalcogenides: Structural Chemistry and Thermoelectric Properties. *J. Materiomics* **2016**, *2*, 131–140.

(6) Clarke, S. J.; Adamson, P.; Herkelrath, S. J. C.; Rutt, O. J.; Parker, D. R.; Pitcher, M. J.; Smura, C. F. Structures, Physical Properties, and Chemistry of Layered Oxychalcogenides and Oxypnictides. *Inorg. Chem.* **2008**, *47* (19), 8473–8486.

(7) Zhao, L. D.; He, J.; Berardan, D.; Lin, Y.; Li, J. F.; Nan, C. W.; Dragoe, N. BiCuSeO Oxyselenides: New Promising Thermoelectric Materials. *Energy Environ. Sci.* **2014**, *7* (9), 2900–2924.

(8) Hiramatsu, H.; Kamioka, H.; Ueda, K.; Ohta, H.; Kamiya, T.; Hirano, M.; Hosono, H. Opto-Electronic Properties and Light-Emitting Device Application of Widegap Layered Oxychalcogenides: LaCuOCh (Ch = Chalcogen) and $La_2CdO_2Se_2$. *Phys. Status Solidi A* **2006**, *203* (11), 2800–2811.

(9) Novitskii, A. P.; Khovaylo, V. V.; Mori, T. Recent Developments and Progress on BiCuSeO Based Thermoelectric Materials. *Nanobiotechnology Reports* **2021**, *16* (3), 294–307.

(10) Zhang, N.; Sun, J.; Gong, H. Transparent P-Type Semiconductors: Copper-Based Oxides and Oxychalcogenides. *Coatings* **2019**, *9* (2), 137.

(11) He, J.; Yao, Z.; Hegde, V. I.; Naghavi, S. S.; Shen, J.; Bushick, K. M.; Wolverton, C. Computational Discovery of Stable Heteroanionic Oxychalcogenides ABXO (A, B = Metals; X = S, Se, and Te) and Their Potential Applications. *Chem. Mater.* **2020**, *32* (19), 8229–8242.

(12) Zhai, Y.; Shim, M. Effects of Copper Precursor Reactivity on the Shape and Phase of Copper Sulfide Nanocrystals. *Chem. Mater.* **2017**, *29* (5), 2390–2397.

(13) Xu, W.; Bony, B. A.; Kim, C. R.; Baeck, J. S.; Chang, Y.; Bae, J. E.; Chae, K. S.; Kim, T. J.; Lee, G. H. Mixed Lanthanide Oxide Nanoparticles as Dual Imaging Agent in Biomedicine. *Sci. Rep.* **2013**, *3* (1), 1–10.

(14) Doussier-Brochard, C.; Chavillon, B.; Cario, L.; Jobic, S. Synthesis of P-Type Transparent LaOCuS Nanoparticles via Soft Chemistry. *Inorg. Chem.* **2010**, *49* (7), 3074–3076.

(15) Schaak, R. E.; Mallouk, T. E. Perovskites by Design: A Toolbox of Solid-State Reactions. *Chemistry of Materials* **2002**, *14* (4), 1455–1471.

(16) Uppuluri, R.; Sen Gupta, A.; Rosas, A. S.; Mallouk, T. E. Soft Chemistry of Ion-Exchangeable Layered Metal Oxides. *Chem. Soc. Rev.* **2018**, *47* (7), 2401–2430.

(17) Alameda, L. T.; Moradifar, P.; Metzger, Z. P.; Alem, N.; Schaak, R. E. Topochemical Deintercalation of Al from MoAlB: Stepwise Etching Pathway, Layered Intergrowth Structures, and Two-Dimensional MBene. *J. Am. Chem. Soc.* **2018**, *140* (28), 8833–8840.

(18) Gopalakrishnan, J. Chimie Douce Approaches to the Synthesis of Metastable Oxide Material. *Chem. Mater.* **1995**, *7* (7), 1265–1275.

(19) Sasaki, S.; Driss, D.; Grange, E.; Mevellec, J.-Y.; Caldes, M. T.; Guillot-Deudon, C.; Cadars, S.; Corraze, B.; Janod, E.; Jobic, S.; Cario, L. A Topochemical Approach to Synthesize Layered Materials Based on the Redox Reactivity of Anionic Chalcogen Dimers. *Angew. Chem., Int. Ed.* **2018**, *130* (41), 13806–13811.
(20) Kodenkandath, T. A.; Lalena, J. N.; Zhou, W. L.; Carpenter, E. E.; Sangregorio, C.; Falster, A. U.; Simmons, W. B.; O'Connor, C. J.; Wiley, J. B. Assembly of Metal-Anion Arrays within a Perovskite Host. Low-Temperature Synthesis of New Layered Copper-Oxyhalides, (CuX)$LaNb_2O_7$, X = Cl, Br. *J. Am. Chem. Soc.* **1999**, *121* (46), 10743–10746.
(21) De Trizio, L.; Manna, L. Forging Colloidal Nanostructures via Cation Exchange Reactions. *Chem. Rev.* **2016**, *116* (18), 10852–10887.
(22) Li, X.; Ji, M.; Li, H.; Wang, H.; Xu, M.; Rong, H.; Wei, J.; Liu, J.; Liu, J.; Chen, W.; Zhu, C.; Wang, J.; Zhang, J. Cation/Anion Exchange Reactions toward the Syntheses of Upgraded Nanostructures: Principles and Applications. *Matter* **2020**, *2* (3), 554–586.
(23) Saruyama, M.; So, Y. G.; Kimoto, K.; Taguchi, S.; Kanemitsu, Y.; Teranishi, T. Spontaneous Formation of Wurzite-CdS/Zinc Blende-CdTe Heterodimers through a Partial Anion Exchange Reaction. *J. Am. Chem. Soc.* **2011**, *133* (44), 17598–17601.
(24) Udayakantha, M.; Handy, J. V.; Davidson, R. D.; Kaur, J.; Villalpando, G.; Zuin, L.; Chakraborty, S.; Banerjee, S. Halide Replacement with Complete Preservation of Crystal Lattice in Mixed-Anion Lanthanide Oxyhalides. *Angew. Chem., Int. Ed.* **2021**, *60* (28), 15582–15589.
(25) Gouget, G.; Pellerin, M.; Pautrot-D'alençon, L.; Le Mercier, T.; Murray, C. B.; Efficient Photoluminescence of Isotropic Rare-Earth Oxychloride Nanocrystals from a Solvothermal Route *Chem. Commun.* **2020**, *56*, 3429–3432.
(26) Kort, K. R.; Banerjee, S. Shape-Controlled Synthesis of Well-Defined Matlockite LnOCl (Ln: La, Ce, Gd, Dy) Nanocrystals by a Novel Non-Hydrolytic Approach. *Inorg. Chem.* **2011**, *50* (12), 5539–5544.
(27) Du, Y. P.; Zhang, Y. W.; Sun, L. D.; Yan, C. H. Atomically Efficient Synthesis of Self-Assembled Monodisperse and Ultrathin Lanthanide Oxychloride Nanoplates. *J. Am. Chem. Soc.* **2009**, *131* (9), 3162–3163.
(28) Udayakantha, M.; Schofield, P.; Waetzig, G. R.; Banerjee, S. A Full Palette: Crystal Chemistry, Polymorphism, Synthetic Strategies, and Functional Applications of Lanthanide Oxyhalides. *J. Solid State Chem.* **2019**, *270*, 569–592.
(29) Templeton, D. H.; Dauben, C. H. Crystal Structures of Rare Earth Oxychlorides. *J. Am. Chem. Soc.* **1953**, *75* (23), 6069–6070.
(30) Ueda, K.; Hosono, H. Crystal Structure of $LaCuOS_{1-x}Se_x$ Oxychalcogenides. *Thin Solid Films* **2002**, *411* (1), 115–118.
(31) Nunotani, N.; Misran, M. R. I. Bin; Inada, M.; Uchiyama, T.; Uchimoto, Y.; Imanaka, N. Structural Environment of Chloride Ion-Conducting Solids Based on Lanthanum Oxychloride. *J. Am. Ceram. Soc.* **2020**, *103* (1), 297–303.
(32) Marsal, A.; Rossinyol, E.; Bimbela, F.; Téllez, C.; Coronas, J.; Cornet, A.; Morante, J. R. Characterisation of LaOCl Sensing Materials Using CO_2-TPD, XRD, TEM and XPS. *Sens. Actuators B: Chem.* **2005**, *109* (1), 38–43.
(33) Powell, A. E.; Hodges, J. M.; Schaak, R. E. Preserving Both Anion and Cation Sublattice Features during a Nanocrystal Cation-Exchange Reaction: Synthesis of Metastable Wurtzite-Type CoS and MnS. *J. Am. Chem. Soc.* **2016**, *138* (2), 471–474.
(34) Mourdikoudis, S.; Liz-Marzán, L. M. Oleylamine in Nanoparticle Synthesis. *Chem. Mater.* **2013**, *25* (9), 1465–1476.
(35) Gao, G.; Tong, L.; Yang, L.; Sun, C.; Xu, L.; Yang, Z.; Wang, P.; Geng, F.; Xia, F.; Gong, H.; Zhu, J. Effect of Hole Effective Mass and Carrier Concentration on the Conductivity of a Transparent P-Type LaCuOS Semiconductor with Good Transmittance in Both Visible

and Mid-Infrared Ranges. *physica status solidi (RRL) – Rapid Research Letters* **2021**, *15* (11), 2100273.
(36) Zhang, N.; Gong, H. P-Type Transparent LaCuOS Semiconductor Synthesized via a Novel Two-Step Solid State Reaction and Sulfurization Process. *Ceram. Int.* **2017**, *43* (8), 6295–6302.
(37) Rudyk, B. W.; Blanchard, P. E. R.; Cavell, R. G.; Mar, A. Electronic Structure of Lanthanum Copper Oxychalcogenides LaCuOCh (Ch=S, Se, Te) by X-Ray Photoelectron and Absorption Spectroscopy. *J. Solid State Chem.* **2011**, *184* (7), 1649–1654.
(38) Zhang, N.; Liu, X.; Annadi, A.; Tang, B.; Gong, H. Highly Conducting P-Type Transparent LnCuOS (Ln = La and Nd) and p-n Junction by Using Ink. *ACS Appl. Electron. Mater.* **2019**, *1* (8), 1605–1615.
(39) Zhang, N.; Liu, X.; Lim, D. B. K.; Gong, H. A New Highly Conductive Direct Gap P-Type Semiconductor $La_{1-x}Y_xCuOS$ for Dual Applications: Transparent Electronics and Thermoelectricity. *ACS Appl. Mater. Interfaces* **2020**, *12* (5), 6090–6096.
(40) Pandey, A.; Jain, G.; Vyas, D.; Irusta, S.; Sharma, S. Nonreducible, Basic La_2O_3 to Reducible, Acidic $La_{2-x}Sb_xO_3$ with Significant Oxygen Storage Capacity, Lower Band Gap, and Effect on the Catalytic Activity. *J. Phys. Chem. C* **2017**, *121* (1), 481–489.
(41) Kim, D.; Park, S.; Kim, S.; Kang, S. G.; Park, J. C. Blue-Emitting Eu^{2+}-Activated LaOX (X = Cl, Br, and I) Materials: Crystal Field Effect. *Inorg. Chem.* **2014**, *53* (22), 11966–11973.
(42) Jain, P. K.; Manthiram, K.; Engel, J. H.; White, S. L.; Faucheaux, J. A.; Paul Alivisatos, A.; Jain, P. K.; White, S. L.; Faucheaux, J. A.; Manthiram, K.; Engel, J. H.; Alivisatos, A. P. Doped Nanocrystals as Plasmonic Probes of Redox Chemistry. *Angew. Chem., Int. Ed.* **2013**, *52* (51), 13671–13675.
(43) Zhao, Y.; Pan, H.; Lou, Y.; Qiu, X.; Zhu, J.; Burda, C. Plasmonic $Cu_{2-x}S$ Nanocrystals: Optical and Structural Properties of Copper-Deficient Copper(I) Sulfides. *J. Am. Chem. Soc.* **2009**, *131* (12), 4253–4261.
(44) Amason, E. K.; Jones, M. H.; Keuk, C.; Ferrence, G. M.; Joslin, E. E.; Bachman, R. E. Synthesis and Characterization of the Complete Series of Chlorine Substituted Cobalt Acetylacetonate Complexes—$[Co(Acac)_x(Acac\text{-}Cl)_{3-x}]$, x = 0–3. *Polyhedron* **2021**, *201*.
(45) Ueda, K.; Takafuji, K.; Hosono, H. Preparation and Crystal Structure Analysis of CeCuOS. *J. Solid State Chem.* **2003**, *170* (1), 182–187.
(46) Orr, M.; Hebberd, G. R.; McCabe, E. E.; Macaluso, R. T. Structural Diversity of Rare-Earth Oxychalcogenides. *ACS Omega* **2022**, *7* (10), 8209–8218.

TABLE OF CONTENTS GRAPHIC